Monitoring the gelation mechanism of resorcinol-formaldehyde gels by dynamic light scattering

*Stewart J. Taylor, Mark D. Haw, Jan Sefcik and Ashleigh J. Fletcher**

Department of Chemical and Process Engineering, University of Strathclyde, Glasgow, G1 1XJ

ABSTRACT: Xerogels and porous materials for specific applications such as catalyst supports, CO_2 capture, pollutant adsorption and selective membrane design require fine control of pore structure, which in turn requires improved understanding of the chemistry and physics of growth, aggregation and gelation processes governing nanostructure formation in these materials. We used time-resolved dynamic light scattering to study the formation of resorcinol-formaldehyde gels through a sol-gel process in the presence of Group I metal carbonates. We showed that an underlying nanoscale phase transition (independent of carbonate concentration or metal type) controls the size of primary clusters during the pre-aggregation phase; while the amount of carbonate determines the number concentration of clusters and, hence, the size to which clusters grow before filling space to form the gel. This novel physical insight, based on a close relationship between cluster size at the onset of gelation and average pore size in the final xerogel results in a well-defined master curve, directly linking final gel properties to process conditions, facilitating the rational design of porous gels with properties specifically tuned for particular applications. Interestingly, while results for lithium, sodium and potassium carbonate fall on the same master curve, cesium carbonate gels have significantly larger average pore size

and cluster size at gelation, providing an extended range of tunable pore size for further adsorption applications.

Introduction

Adsorption applications such as catalyst supports,[1] carbon capture,[2] hydrogen storage,[3] soil remediation,[4] water purification,[5] fuel cell[6] and electrochemical processes,[7] and the design of selective membranes[8] all require fine control of the properties of porous materials, in particular pore sizes, size distributions, and connectivity. Such materials are often made using sol-gel processes, where chemical and physical interactions in solution lead to nucleation, growth and aggregation of clusters and eventual formation of porous solid gels when clusters contact each other to fill space. Our understanding of such aggregation and gelation processes, especially when both chemical reactions, such as polymerisation, and physical effects, such as nanoscale phase separation, are occurring simultaneously, on competing timescales and lengthscales, remains limited. Hence, design and manufacture of bespoke gel materials for specific applications, with pore sizes and other properties easily determined through control of process conditions, is a challenge. In this paper we provide a novel physical insight into the relationship between size and number of primary clusters and final gel properties for one class of porous materials, resorcinol-formaldehyde (RF) gels. This improved understanding of the chemical and physical processes leading to gel formation facilitates the rational design of porous gels with properties specifically tuned for particular applications.

RF gels were first prepared by Pekala in 1989.[9] They were formed through the polycondensation reaction of resorcinol and formaldehyde, in the presence of a base, as part of a sol-gel process. The dried gels had properties of low density, large surface area and high pore volume, as well as

becoming electrically conductive, through pyrolysis which has seen them become potential materials for many of the applications stated above. The proposed reaction mechanism for RF polymerization occurs in two stages (as outlined in Scheme 1). Resorcinol and formaldehyde react to form substituted resorcinol, or the hydroxymethyl derivative, with mono-, di- and tri-substituted resorcinol being produced. This is followed by polycondensation of these intermediates to form growing oligomers, which subsequently make up the clusters that compose the gel structure. The reaction is commonly carried out in the presence of a base, typically sodium carbonate; however, alternative cations such as lithium and potassium[10,11] have been used, as well as hydroxide[10] and hydrogencarbonate[12] anions. It has been shown that resorcinol and formaldehyde will react slowly by themselves, but the resulting product is an apparently non-porous powder.[13] Similarly, in the presence of ammonium carbonate (a non-metallic base), a comparable non-porous product is formed.[13] Ammonium carbonate will decompose in the system producing ammonia, which will subsequently react with F. However, as the ammonium carbonate is added in such small quantities, less than 1 % of the available F should react in this way and have little impact on the gel formation. This suggests that while the base is important, the metal also plays a role in the gelation process, determining the final porous characteristics of the materials.

Since the discovery of RF gels,[9] it has become common within the literature to refer to the added base as a catalyst.[14, 15] This is primarily due to its role in speeding up the formation of the final gel product. However, the metal carbonate appears to decompose during the gel formation reaction and is, therefore, not recoverable at the end of the process. In addition, the complicated role the metal plays in the formation of the gel structure makes it more than just a catalyst. Hence, the added base will be referred to as simply carbonate (C) from here on in.

During the years since they were first synthesized, much work has been carried out on RF gels.[14, 15] As previously noted, the metal counter-ion of the carbonate plays an important role in determining the porous properties of the dried gels. However, there are several other variables in the sol-gel reaction that can be altered in order to change the porous nature of the resulting gels. Some of these variables include total solids content (also referred to as the resorcinol to water ratio R/W in g/ml), resorcinol to formaldehyde molar ratio (R/F), resorcinol to carbonate molar ratio (R/C) and initial solution pH. In this regard, R/C and pH are closely related in RF gel synthesis.

Lin and Ritter[16] tried to decouple the relationship between R/C and pH, by fixing the R/C at 50, while altering the pH through the addition of nitric acid. However, the acid added will react with the carbonate present, reducing the concentration of acid or base available to participate in the sol-gel process.

There have been many findings indicating that initial pH is vitally important to the final properties of the gel.[14, 15] Much work has shown that gel synthesis in the presence of a base will typically only give a viable gel structure within the limited pH range of 5.5 – 7.5.[15, 17] More basic pH values give a non-porous structure,[16] while pH values less than 5.5 give a very long gelation time.[18] However, further lowering of the pH to within the range of approximately 1 – 4, through the addition of an acid instead of a base, will once more promote viable gel formation and reduce gelation times.[18, 19] A pH of less than 0.8 will cause precipitation of the reactants.[15]

These useable ranges can be attributed to the requirements of the two stages in the polymerization process. The initial addition reaction can be favored by basic conditions, to abstract a proton from R, or by acidic conditions, wherein F is protonated, both of which

promote the reaction between R and F. Consequently, when the pH is out with the stated ranges, the addition reaction is slowed and the gel time will increase.[18] The subsequent condensation reaction is also favored by acidic conditions. If the initial pH is too basic, there will be a lack of condensation reactions and the resulting gel structure will be very weak. This will result in the total collapse of the porous structure during drying, leading to a non-porous product.[16] The initial system pH can also have a secondary impact on the growth of polymer chains. High pH values resulting from low R/C values will lead to highly branched polymer chains. Conversely, low pH values as a result of high R/C ratios will produce less branched polymer chains.[17]

Altering the solids content, i.e. total resorcinol, formaldehyde and carbonate, can have a substantial impact on the properties of the dried gel.[14] The effective dilution of the reactant solution, by decreasing the solids content, gives rise to larger gaps between the growing clusters. This leads to an increase in the pore size and a corresponding decrease in surface area.[11] Tamon *et al*.[20] reported that with high solids content, the porosity of the gel was monodisperse, i.e. all pores were of a similar size. Conversely, low solids content produced polydisperse porosity with multiple pore sizes observed.

From the first synthesis of RF gels, resorcinol and formaldehyde have most commonly been combined in the stoichiometric proportion of 1:2 giving an R/F ratio of 0.5.[9] Increasing the formaldehyde concentration present, to give a 1:3 ratio, leads to the observation of much larger final clusters.[21]

Dynamic Light Scattering (DLS) has previously been used to study the formation of RF gels. However, these studies have been limited, in that they focus on only the most commonly used

base, sodium carbonate. Yamamoto *et al.*[22] observed that for a given resorcinol to water ratio, the growth of primary clusters was highly dependent on the carbonate concentration in the initial RF solution. They showed that as resorcinol: carbonate molar ratio (R/C) increased; the growth rate slowed such that, at a given time, high R/Cs gave a smaller cluster size than low R/C values. Conversely, Gaca and Sefcik[23] argued that in the early gelation stages, primary cluster size changed minimally as the carbonate concentration was altered. Instead, the process was thermodynamically driven and primary cluster growth rates were essentially independent of R/C values.

The aim of this work was to study the influence of four Group I metal carbonates, at various R/C ratios, on the RF sol-gel reaction and the subsequent properties of the dried gels. This was achieved through the use of DLS to monitor primary cluster growth in the initial stages of the gelation process, followed by characterization through low temperature nitrogen adsorption/desorption measurements of the final xerogels, allowing direct comparison between gel formation and the resulting sample textural properties.

Experimental

Materials and Synthesis

The composition of the RF solution was determined using the molar ratios of resorcinol to carbonate (R/C) and resorcinol to formaldehyde (R/F). The total solids content of the gel, i.e. resorcinol, formaldehyde and carbonate, was kept constant at 20 % weight by volume. A gel volume of 60 ml was used in each case; corresponding to a solid mass of 12 g. R/C was varied between 100 and 600 for each of the carbonates used, while R/F was fixed at 0.5.

Resorcinol (ReagentPlus, 99 %), aqueous formaldehyde solution (37 wt. % formaldehyde, stabilised with 10-15 % methanol), lithium carbonate (purum, ≥99 %), sodium carbonate (anhydrous, ≥99.5 %), potassium carbonate (anhydrous powder, 99.99 %) and caesium carbonate (ReagentPlus, 99 %) were all used as purchased from SigmaAldrich.

For a chosen carbonate and R/C ratio, the required resorcinol was weighed out and placed in a sealable 500 ml jar with 50 ml of deionised water (produced in house as required using a Millipore Elix 5 system), and magnetically stirred until completely dissolved. The carbonate was weighed out and added to the resorcinol solution with continued stirring, again until completely dissolved. The required volume of formaldehyde solution and additional deionised water, to give the total volume of 60 ml, was added to the jar, which was sealed and allowed to stir uninterrupted for 30 minutes. At the end of this stirring period, the initial pH of the solution was recorded (Hanna pH 20 meter, fitted with an HI-1110B pH electrode) and the sealed jars placed in an oven preheated to 85 ± 5 °C until gelation occurred. Gelation times were monitored for each of the metal carbonates used at all of the chosen R/C ratios. Gelation was determined by periodically tilting the jars to a 45° angle until no flow was observed. To allow for curing of the newly formed gel, the samples were left at 85 ± 5 °C for three days.

Water entrained within the cured gel network was removed through solvent exchange, by shaking the cured gel in 180 ml of acetone (ACS reagent, ≥99.5 %, Sigma Aldrich) for three days at room temperature. This step reduced shrinkage of the structure during drying, especially for high R/C gels. Subsequently, the gels were dried under vacuum at 85 °C for two days to produce the final xerogel product.

Xerogel Characterisation

Surface area and porosity measurements were performed on a Micromeritics ASAP 2420, using nitrogen adsorption/desorption measurements. Approximately 0.5 g of the dried gel was accurately weighed into a sample tube, which was attached to a degas port of the equipment. After securing a heating mantle around the tube, the sample was evacuated by attached vacuum pump first to 5 mmHg, then to 10 μmHg, while being heated to 50 °C. After being held at these conditions for 30 minutes, the temperature was ramped to 110 °C and this temperature maintained for 120 minutes. On completion of the degas cycle, the sample and tube were reweighed to determine the mass lost. An analysis port was prepared and analysis performed at -196 °C, maintained by liquid nitrogen, and consisting of 40 point adsorption and 30 point desorption cycles.

Brunauer-Emmett-Teller (BET) theory[24] was applied to the adsorption branch of the acquired nitrogen uptake isotherm,

resulting in a linear plot between the relative pressures (p/p_0) of 0.05 and 0.3. This allowed calculation of the BET surface area (S_{BET}) for each of the gel samples. Similarly, the Barrett-Joyner-Halenda (BJH) method[25] was applied to the desorption branch of the isotherm. This generated a pore size distribution for the gel samples and allowed calculation of the average pore size.

Dynamic Light Scattering

DLS experiments were carried out on an ALV/CGS-3 Compact Goniometer System in conjunction with an ALV/LSE-5004 Multiple Tau Digital Correlator. The laser used had wavelength, λ, 632.8 nm, with a scattering angle, θ, of 90°. After measuring the solution pH, portions of the solution were passed through a 0.2 μm pore size syringe filter (Whatman

Puradisc) into 11 borosilicate glass cells with 10 mm diameter and height of 75 mm (Fisher Scientific). All 11 cells were then sealed with a cap, and 10 were transferred to an oven set to 85 ± 5 °C, while the 11th cell was taken for immediate analysis and designated t = 0. Making use of the predetermined gel times, further cells were removed from the oven at intervals of 10 % of these times, upon which they were rapidly quenched to room temperature and analysed.

For each experimental time point, the digital correlator generated an autocorrelation function of the scattered light intensity. When the autocorrelation function decay followed an exponential time dependence, indicative of free Brownian motion of the species present, the cumulant method[26] was applied in order to estimate the initial decay rate, $\Gamma (s^{-1})$. Subsequently, the mean diffusion coefficient, D, was calculated:

$$\Gamma = Dq^2$$

where q is the scattering vector magnitude:

$$q = \frac{4\pi}{\lambda} sin\frac{\theta}{2}$$

From this, the Stokes-Einstein equation[27, 28] can be used to calculate the mean hydrodynamic radius, R_H:

$$R_H = \frac{k_b T}{6\pi\mu D}$$

where k_B is the Boltzmann constant, T is absolute temperature and μ is the dynamic viscosity. For all calculations, μ was assumed to be that of pure water at the experimental temperature.

Results and Discussion

Gelation times as determined in this work are 35 minutes for R/C 100, 43 minutes for R/C 200, 55 minutes for R/C 300, 65 minutes for R/C 400, 80 minutes for R/C 500 and 120 minutes for R/C 600. It was found that for an equivalent R/C the gelation time for each of the carbonates was identical, while it is clear that increasing R/C leads to increased gelation times. This contrasts with Morales-Torres *et al.* who found that for a fixed R/C of 300, and thermal regime of one day at room temperature followed by heating to 50 °C, the gel time increased over the Group I metal series, with lithium giving the shortest time and caesium the longest.[29] However, they do agree with those of Job *et al.* who also found that gel time increased with increasing R/C.[30]

It should be noted that the sample synthesized using caesium carbonate with R/C 600 failed to gel within a time frame experimentally viable for DLS to be conducted.

For the gel times obtained, intervals of 10 % of the total gel time were chosen with which to run DLS measurements, as opposed to a fixed time interval. This allowed for direct comparison between all of the gel compositions at an equivalent point in the gelation process.

Upon analysis of the gelling samples, the experimental equipment provided two sets of raw data for each measurement time point, both of which provide valuable information on the gelation process. The first of these data sets were autocorrelation functions for each sample, while the second contained the corresponding scattered light intensities.

Figure 1 shows the normalized autocorrelation functions obtained over the entire gelation period for both sodium and cesium carbonate, with a fixed R/C of 100 in both cases (see Supporting Information for the corresponding lithium and potassium data, as well as those for sodium carbonate at both R/C 400 and 600).

Initially, the decay of the autocorrelation function demonstrates a strictly exponential dependence on time. This corresponds to free Brownian motion and suggests that, while the primary clusters are growing, they are moving without obstruction, or intercluster interaction. As the experimental time increases (for example t = 80 %, i.e. 28 minutes for R/C 100), the shape of the autocorrelation function changes, moving away from a purely exponential decay and introducing a small secondary decay. This implies that further species with slower dynamics are now present, suggesting that aggregation or networking of primary clusters has begun and their movement is beginning to become hindered. In order to clearly discriminate between aggregation and networking of the clusters, more detailed models of cluster populations evolving over time and fitted to the measured autocorrelation functions would be required.[31]

At times very close to, and at, the total gel time, the autocorrelation function fails to decay completely, becoming non-ergodic. This feature is indicative of a predominantly formed gel structure. The small initial decay that remains suggests that some degree of motion is still possible and the gel has not become completely rigid. Indeed, Job *et al.* found that between 24 and 48 hours of aging the gel was required to give a stable pore texture. [18] It is possible that these residual movements are caused by polymeric branches that have still to connect completely with the formed clusters, resulting in additional decay contributions to the autocorrelation functions. However, these contributions are likely to be slower than those of the corresponding diffusivity of primary clusters.[31] Figure 2 illustrates each of these profile types on a log-log scale, showing how, earlier in the gelation process, the profile follows the exponential decay. At later times, it clearly deviates away from that of a purely exponential profile.

As stated above, the hydrodynamic radius of the growing clusters can be determined by the cumulant method. This analysis was limited to only those autocorrelation functions showing

purely exponential decay, where the clusters are moving freely. As the clusters start aggregating or networking near gelation, their movement is no longer free and the exponential decay is lost. The combination of these factors means that the true hydrodynamic radius of clusters can no longer be determined.

Figure 3 shows the hydrodynamic radii determined from the initial decay of the autocorrelation function for each carbonate at all R/C ratios. It can be seen that, in all cases, there is a period of time wherein the hydrodynamic radii are less than 1 nm and do not grow. This size compares with the 0.4 nm hydrodynamic radius for a hydrated resorcinol molecule,[23] suggesting that only hydroxymethyl derivatives are present at this time.

This delay in growth is the consequence of the time taken for samples to heat up after being placed in the oven. After measurement of the temperature of each individual sample on removal from the oven and before quenching, during experimental runs using sodium carbonate at R/C ratio of 100, it was found that growth began when the samples reached approximately 55 °C. As such, preheating of the initial solution to 55 °C eliminates this delay (see Supporting Information, Figure SI3 and SI4).

When comparing the growth of clusters produced when using lithium, sodium and potassium carbonate (Figure 3a), it can be seen that the hydrodynamic radii fall into an overlapping narrow band. This indicates that the growth of the clusters is virtually independent of the R/C ratio or metal carbonate used. The maximum pre-gelation hydrodynamic radius does, however, show a dependence on R/C, with the maximum hydrodynamic radius increasing as R/C ratio increases. This trend is shown in Figure 4.

In contrast, the cluster growth in the presence of cesium carbonate is much different to the corresponding lithium, sodium and potassium carbonate systems (Figure 3b). The growth is no longer consistent across the R/C spectrum, with low R/C ratio clusters growing faster than those with higher R/C. Despite identical thermal conditions, the time delay before the onset of growth also varies significantly, with longer times for the higher R/C systems, ranging from less than 15 minutes for R/C 100, to more than 25 minutes for R/C 500. It should also be noted that for a given R/C ratio, the maximum calculated pre-gelation hydrodynamic radius is much larger for cesium carbonate systems when compared with the lithium, sodium and potassium carbonate counterparts, as seen in Figure 4.

The time dependent scattered light intensities, as taken from the digital correlator at each measurement time point, are shown in Figure 5 (see Supporting Information for the corresponding lithium and potassium carbonate results). Examination of this data provides further information on the cluster growth process. In the case of lithium, sodium and potassium, the results are once more very similar. In general, for a given time the scattered light intensity decreases with increasing R/C. As hydrodynamic radius measurements indicate that, at any given time, cluster size is very similar for all R/C values; this decrease in scattered intensity implies a decrease in the number concentration of scatterers, i.e. clusters. An increase in R/C ratio therefore leads to a decrease in the number concentration of clusters at a given time. A sample made with an R/C of 100 generates many more clusters than an R/C 600 sample, yet they grow at the same rate.

The scattered light intensities recorded for gels made with cesium carbonate follow the same general trend as the other metals, with increasing R/C resulting in decreasing intensity at a given time. However, changes in the scattered intensity at a given time for the different R/C ratios are

due not only to changes in the cluster number concentration but also in cluster size. Whilst still being monodisperse, the hydrodynamic radii of the clusters in these cesium carbonate gels, at the different R/C ratios, are not consistent at a given time, implying a dependence on R/C. As a result, it was not possible to decouple the relationship between cluster size and their number concentration in cesium carbonate systems.

Surface area and porosity measurements were carried out on each of the dried gels. Example subsets of the adsorption/desorption isotherms and pore size distributions obtained are shown in Figure 6 (see Supporting Information for results for lithium and potassium carbonate gels).

Consistent with observations from hydrodynamic radii obtained by DLS, it can be seen that in the case of both isotherms and pore size distributions, the results for lithium, sodium and potassium are very similar, while those for cesium differ greatly. However, there are discernible trends that apply to all four of the cations studied. As shown by the isotherm data, for each carbonate, increasing the R/C ratio leads to a general increase in the amount of nitrogen adsorbed. This is accompanied by a shifting of the hysteresis loop to higher relative pressures. These observations are indicative of an increase in both pore diameter and total pore volume, as supported by the pore size distributions. At a given R/C, the equivalent cesium gels show a greater nitrogen uptake than the other carbonates. This is mirrored in the greatly increased pore size. The results obtained for cesium carbonate at R/C 500 do not follow the trends established by the other cesium gels; the nitrogen uptake is much lower than expected, as is the pore volume. At high R/C values, the pre-solvent exchanged, cured cesium gels are much softer than those of the other carbonates used. This leads to greater shrinkage during the drying phase, causing a reduction in pore volume. In conjunction with the R/C 600 cesium sample failing to gel, this suggests that the upper R/C limit to produce feasible cesium gels has been reached.

Further details on the properties of each gel are given in Table 1. The initial solution pH, as measured at the end of the 30 minute stirring period, is included for reference. For each carbonate there are several trends that agree with the literature described above. As expected, initial pH decreases with increasing R/C and is consistent between the four cations, with a given R/C resulting in approximately the same pH. Average pore sizes increase with increasing R/C, agreeing with the visual analysis of the adsorption/desorption isotherms. The values for lithium, sodium and potassium compare well, with a large increase for the corresponding cesium gels. Once more, this agrees with examination of the pore size distributions. This increase in pore size gives an associated decrease in the BET surface area.

By combining the data on the maximum pre-gelation hydrodynamic radii of clusters and the average pore size of the gels it can be seen that there is a clear correlation between these two values, where all data for lithium, sodium and potassium fall on a single Master Curve. Figure 7 shows this Master Curve, and the range of values of pore size accessible in these systems. As expected from analysis of the above results, the cesium gels do not conform to the Master Curve exhibited by the other Group I metal carbonates used. However, the data follows the same trend, with the cesium carbonate results following a similar dependence between the average pore size and maximum pre-gelation size of clusters. In Figure 7b we can see that these xerogels can provide a wide range of average pore sizes, which can be systematically tailored for the number of potential applications as required.

It is likely that this correlation will hold with regard to average pore diameter vs. final particle size of the dried gel. However, electron microscopy imaging has not been performed at this time, preventing a definitive conclusion from being drawn.

The ordering of the metals in this work, where lithium = sodium = potassium < cesium with regard to cluster size produced appears to follow a Hofmeister like series, all be it in reverse order. Hofmeister found that lithium > sodium > potassium at salting out egg protein from solution, by stabilizing the protein molecules and making them less soluble.[32] Our observations appear to show that lithium, sodium and potassium have approximately equal ability to stabilize the RF colloidal suspension by destabilizing the oligomers and increasing their solubility, resulting in small clusters. On the other hand, the larger, more hydrated cesium cation[33] appears to be less able to stabilize the colloidal suspension, making the oligomers less soluble and leading to larger clusters.

Previous literature on the formation of RF gels has been mainly focused on the microphase separation mechanism.[10, 34, 35] As resorcinol becomes substituted and the subsequent condensation polymerization proceeds, a complex mixture of water, alcohol, salt and organic oligomers is formed. As the oligomer length increases, the miscibility of the chain with water decreases, leading to demixing of the components into two microphases.

However, the classical microphase separation scenario results in two interpenetrating microphases, which is inconsistent with DLS observations of freely diffusing primary clusters. Therefore, another kind of nanoscale phase transition needs to be considered, such as mesostructured liquid phase formation, where a single liquid phase consists of the bulk solution containing localized liquid-like regions of the organic species.[23, 36]

The DLS results obtained here appear to support this theory. In the case of lithium, sodium and potassium, the primary cluster size growth in the initial pre-gelation stages is independent of the metal cation and R/C ratio used. This implies the formation of similar oligomeric species in all

cases, which form monodisperse clusters of the observed hydrodynamic radius, surrounded by the bulk solution containing water/resorcinol/formaldehyde. This process is depicted schematically in Figure 8. The schematic depicts primary clusters as spherical for clarity, as the exact shape and internal structure of the clusters is not yet known. Primary clusters can contain variously branched oligomers which are likely to be physically aggregated while also undergoing further polymerization. We do not believe that clusters are individual polymeric species, since their size has been found to be independent of R and F concentration at a given carbonate concentration, and therefore appears to be controlled thermodynamically rather than by kinetics of the polymerization process.[23]

In reality, these primary clusters can have any arbitrary shape (be it irregular and/or fractal). However, they do have a well-defined hydrodynamic radius, as demonstrated here, and corresponding occupied volume.[37] These clusters are then subject to further physical aggregation which leads to formation of a 3D network and in turn gelation, as the total volume occupied by clusters reaches a critical value. Formation of the physically aggregated 3D network may be accompanied and/or followed by chemical bonding due to underlying polymerization processes.

The lower number concentration of clusters associated with higher R/C ratios will have to grow larger before they reach this critical volume. Conversely, the large number concentration of clusters produced at low R/C ratios will pass this volume at much smaller sizes. As all clusters grow at the same rate, the larger the clusters have to grow before reaching this volume will result in an increasing gelation time as observed.

While it is theoretically possible for differently branched polymers to have the same hydrodynamic radius, for this to happen here primary cluster size would need to be controlled by

polymerization kinetics. However this is not the case here, with this work showing that the size of primary clusters appears to be thermodynamically controlled. Therefore, it is likely that primary clusters are formed by nanoscale phase transition involving RF oligomers which are physically aggregated. As such, formation of 3D networks in various molecular and colloidal systems has been demonstrated to be the result of physical aggregation of primary particles or clusters.[38, 39, 40]

The schematic differs from the model proposed by Yamamoto *et al.*[22, 41] in several key aspects. Their model proposed that both size and growth rate of clusters were driven by chemical reaction kinetics, being highly dependent on the R/C used. The higher the carbonate concentration used, the greater the apparent cluster growth rate became. However, in their work non-exponential autocorrelation functions were analyzed to determine the apparent cluster sizes under conditions that were likely to be in the regime of aggregation and networking, where cluster mobility is severely hindered and, therefore, cluster sizes cannot be reliably determined. In contrast, we propose that primary cluster size is determined by nanoscale phase transition and is, therefore, as previously stated thermodynamically controlled, rather than determined by reaction kinetics. However, the number concentration of primary clusters is kinetically controlled through reaction kinetics, where higher carbonate concentrations results in faster production of the substituted resorcinol and resulting oligomers, leading to a larger number of primary clusters.

The results presented here are subsequently inconsistent with the mechanism first proposed by Pekala and Kong,[42] that of the "autocatalytic growth" mechanism. Through this mechanism, Pekala and Kong intimated that with increasing carbonate concentration came an increasing number of more reactive substituted resorcinol molecules and, therefore, a greater number of the initial bridged dimer condensation products. The quadruple functionality on these dimer species

increased the probability that they would react further to produce larger oligomers. The greater number of dimers produced by the higher carbonate concentration therefore led to a faster reaction rate, with lower carbonate concentration leading to a correspondingly slower reaction. The results obtained in this work suggest that this is not the case, with cluster growth proceeding at the same rate, independent of the carbonate concentration.

Conclusions

From the results obtained through DLS, it was found that lithium, sodium and potassium exhibited very similar trends in size and growth kinetics of primary clusters. The cluster growth kinetics were found to be very similar for all samples studied, independent of the metal carbonate and R/C used. This suggests that clusters have the same mean size at a given time until the sample nears the gelation time, indicative of a thermodynamically controlled process of primary cluster formation. The R/C ratio determines the number concentration of these clusters present, with an increase in the quantity of clusters as R/C decreases. A greater number concentration of clusters results in the clusters reaching a critical volume more quickly, which, in turn, leads to smaller final pre-gelation cluster sizes and shorter gelation times. This is consistent with the pore sizes observed, with smaller diameters corresponding to lower R/C values.

These results lend weight to a mechanism consisting of a nanoscale phase transition, such as mesostructured liquid phase formation. With mesostructured liquid phase formation, the growing oligomers reach their miscibility limit and the solution undergoes a phase transformation, resulting in the formation of primary clusters dispersed in the bulk aqueous solution. This phase transition is dependent on the size of the oligomers produced by the condensation reaction, and

so occurs once a certain temperature and/or composition threshold is reached, irrespective of R/C.

This reinforces the point that the metal cation species plays an important role in the gel formation process. However, the high degree of similarity in the results of lithium, sodium and potassium, coupled with the vastly different results for cesium means the understanding of this role is still not complete. Cesium carbonate shows different behavior, where pre-gelation cluster sizes are significantly larger than those of the other metals studied at equivalent R/C ratios. This leads to greatly increased pore sizes. The metal cations appear to follow a Hofmeister like series, with the smaller, less hydrated lithium, sodium and potassium cations giving smaller clusters than the larger, more hydrated cesium cation.

However, the mechanism developed here means that the average pore sizes of the resulting xerogels can be precisely tailored, allowing for the development of numerous applications for these materials. Use of cesium carbonate gives access to a region of properties which are unobtainable using lithium, sodium or potassium carbonate. While the pore sizes obtained for these three metals are ideal for gas phase applications, the larger pores of cesium gels fall into the range required for aqueous phase processes. This means that the number and scope of potential applications for these materials is significantly expanded.

ASSOCIATED CONTENT

Supporting Information. Autocorrelation functions for lithium and potassium carbonate at R/C 100, autocorrelation functions for sodium carbonate at R/C 400 and 600, temperature profile for sodium carbonate at R/C 100, hydrodynamic radii for sodium carbonate when preheated to 55 °C, scattered light intensities for lithium and potassium carbonate, adsorption/desorption

isotherms for lithium and potassium carbonate, pore size distributions for lithium and potassium carbonate (PDF). This material is available free of charge via the Internet at http://pubs.acs.org.

AUTHOR INFORMATION

Corresponding Author

*e-mail: ashleigh.fletcher@strath.ac.uk

Notes

The authors declare no competing financial interest.

ACKNOWLEDGMENT

The authors acknowledge financial support from The University of Strathclyde for SJT.

ABBREVIATIONS

R, Resorcinol; F, Formaldehyde; C, Metal Carbonate; R/C, Resorcinol to Carbonate molar ratio; R/F, Resorcinol to Formaldehyde molar ratio; DLS, Dynamic Light Scattering; BET, Brunauer-Emmett-Teller; BJH, Barrett-Joyner-Halenda.

REFERENCES

(1) Rodrigues, E. G.; Pereira, M. F. R.; Orfao, J. J. M. Glycerol oxidation with gold supported on carbon xerogels: Tuning selectivities by varying mesopore sizes. *Appl. Catal., B* **2012**, *115-116*, 1-6.

(2) Luo, C.; Zheng, Y.; Zheng, C.; Yin, J.; Qin, C.; Feng, B. Manufacture of calcium-based sorbents for high temperature cyclic CO_2 capture via sol-gel process. *Int. J. Greenh. Gas Control* **2013**, *12*, 193-199.

(3) Zubizarreta, L.; Menéndez, J. A.; Job, N.; Marco-Lozar, J. P.; Pirard, J. P.; Pis, J. J.; Linares-Solano, A.; Cazorla-Amorós, D.; Arenillas, A. Ni-doped carbon xerogels for H_2 storage. *Carbon* **2010,** *48*, 2722-2733.

(4) Tang, J.; Zhu, W.; Kookana, R.; Katayama, A. Characteristics of biochar and its application in remediation of contaminated soil. *J. Biosci. Bioeng.* **2013**, *116*, 653-659.

(5) Porada, S.; Weinstein, L.; Dash, R.; van der Wal, A.; Bryjak, M.; Gogotsi, Y.; Biesheuvel, P. M. Water desalination using capacitive deionization with microporous carbon electrodes. *ACS Appl. Mater. Interfaces* **2012,** *4*, 1194-1199.

(6) Jin, H.; Zhang, H.; Ma, Y.; Xu, T.; Zhong, H.; Wang, M. Stable support based on highly graphitic carbon xerogel for proton exchange membrane fuel cells. *J. Power Sources* **2010,** *195*, 6323-6328.

(7) Pekala, R. W.; Farmer, J. C.; Alviso, C. T.; Tran, T. D.; Mayer, S. T.; Miller, J. M.; Dunn, B. Carbon electrodes for electrochemical applications. *J. Non-Cryst. Solids* **1998,** *225*, 74-80.

(8) Magueijo, V. M.; Anderson, L. G.; Fletcher, A. J.; Shilton, S. J. Polysulfone mixed matrix gas separation hollow fibre membranes filled with polymer and carbon xerogels. *Chem. Eng. Sci.* **2013**, *92*, 13-20.

(9) Pekala, R. W. Organic aerogels from the polycondensation of resorcinol with formaldehyde. *J. Mater. Sci.* **1989,** *24*, 3221-3227.

(10) Job, N.; Gommes, C. J.; Pirard, R.; Pirard, J.-P. Effect of the counter-ion of the basification agent on the pore texture of organic and carbon xerogels. *J. Non-Cryst. Solids* **2008,** *354*, 4698-4701.

(11) Fairén-Jiménez, D.; Carrasco-Marín, F.; Moreno-Castilla, C. Porosity and surface area of monolithic carbon aerogels prepared using alkaline carbonates and organic acids as polymerization catalysts. *Carbon* **2006,** *44*, 2301-2307.

(12) Horikawa, T.; Hayashi, J.; Muroyama, K. Controllability of pore characteristics of resorcinol-formaldehyde carbon aerogel. *Carbon* **2004,** *42*, 1625-1633.

(13) Anderson, L. The Effect of the Catalyst on the Formation of RF Xerogels. Ph.D. Thesis, University of Strathclyde, Glasgow, 2014.

(14) Al-Muhtaseb, S. A.; Ritter, J. A. Preparation and properties of resorcinol-formaldehyde organic and carbon gels. *J. Adv. Mater.* **2003,** 15, 101-114.

(15) El Khatat, A. M.; Al-Muhtaseb, S. A. Advances in tailoring resorcinol-formaldehyde organic and carbon gels. *J. Adv. Mater.* **2011,** 23, 2887-2903.

(16) Lin, C.; Ritter, J. A. Effect of synthesis pH on the structure of carbon xerogels. *Carbon* **1997,** *35*, 1271-1278.

(17) Job, N.; Pirard, R.; Marien, J.; Pirard, J.-P. Porous carbon xerogels with texture tailored by pH control during sol-gel process. *Carbon* **2004,** *42*, 619-628.

(18) Job, N.; Panariello, F.; Marien, J.; Crine, M.; Pirard, J.-P.; Léonard, A. Synthesis optimization of organic xerogels produced from convective air-drying of resorcinol–formaldehyde gels. *J. Non-Cryst. Solids* **2006**, *352*, 24-34.

(19) Mulik, S.; Sotiriou-Leventis, C.; Leventis, N. Time-Efficient Acid-Catalyzed Synthesis of Resorcinol−Formaldehyde Aerogels. *Chem. Mater.* **2007**, *19*, 6138-6144.

(20) Tamon, H.; Ishizaka, H.; Mikami, M.; Okazaki, M. Porous structure of organic and carbon aerogels synthesized by sol-gel polycondensation of resorcinol with formaldehyde. *Carbon* **1997,** *35*, 791-796.

(21) Petričević, R.; Glora, M.; Fricke, J. Planar fibre reinforced carbon aerogels for application in PEM fuel cells. *Carbon* **2001,** *39*, 857-867.

(22) Yamamoto, T.; Yoshida, T.; Suzuki, T.; Mukai, S. R.; Tamon, H. Dynamic and static light scattering study on the sol-gel transition of resorcinol-formaldehyde aqueous solution. *J. Colloid and Interface Sci.* **2002,** *245*, 391-396.

(23) Gaca, K. Z.; Sefcik, J. Mechanisms and kinetics of nanostructure evolution during early stages of resorcinol-formaldehyde polymerization. *J. Colloid and Interface Sci.* **2013,** *406*, 51-59.

(24) Brunauer, S.; Emmett, P. H.; Teller, E. Adsorption of gases in multimolecular layers. *J. Am. Chem. Soc.* **1938,** *60*, 309-319.

(25) Barrett, E. P.; Joyner, L. G.; Halenda, P. P. The determination of pore volume and area distributions in porous substances. I. computations from nitrogen isotherms. *J. Am. Chem. Soc.* **1951,** *73*, 373-380.

(26) Finsy, R. Particle sizing by quasi-elastic light scattering. *Adv. Colloid Interface Sci.* **1994,** *52*, 79-143.

(27) Einstein, A. On the movement of small particles suspended in stationary liquids required by the molecular theory of heat. *Ann. der Physik 1905***,** *17*, 549-560.

(28) Stokes, G. G. On the effects of the internal friction of fluids on the motion of pendulums. *Cambridge Philos. Trans.* **1851,** *9*, 8-106.

(29) Morales-Torres, S.; Maldonado-Hodar, F. J.; Perez-Cadenas, A. F.; Carrasco-Marin, F. Textural and mechanical characteristics of carbon aerogels synthesized by the polymerization of resorcinol-formaldehyde using alkali carbonates as basification agents. *Phys. Chem. Chem. Phys.* **2010,** *12*, 10365-10372.

(30) Job, N.; Panariello, F.; Crine, M.; Pirard, J.-P.; Léonard, A. Rheological determination of the sol–gel transition during the aqueous synthesis of resorcinol-formaldehyde resins. *Colloid. Surface. A* **2007**, *293*, 224-228.

(31) Sandkühler, P.; Lattuada, M.; Wu, H.; Sefcik, J.; Morbidelli, M. Further insights into the universality of colloidal aggregation. *Adv. Colloid Interfac.* **2005**, *113*, 65-83.

(32) Hofmeister, F. About the science of the effect of salts. *Arch. Exp. Pathol. Pharmakol.* **1888**, *24*, 247-260.

(33) Persson, I. Hydrated metal ions in aqueous solution: How regular are their structures? *Pure Appl. Chem.* **2010**, *82*, 1901-1917.

(34) Pekala, R. W.; Schaefer, D. W. Structure of organic aerogels. 1. Morphology and scaling. *Macromolecules* **1993,** *26*, 5487-5493.

(35) Schaefer, D. W.; Pekala, R.; Beaucage, G. Origin of porosity in resorcinol-formaldehyde aerogels. *J. Non-Cryst. Solids* **1995,** *186*, 159-167.

(36) Jawor-Baczynska, A.; Moore, B. D.; Lee, H. S.; McCormick, A. C.; Sefcik, J. Population and size distribution of solute-rich mesospecies within mesostructured aqueous amino acid solutions. *Faraday Discuss.* **2013**, *167*, 425-440.

(37) Sandkühler, P.; Sefcik, J.; Morbidelli, M. Scaling of the Kinetics of Slow Aggregation and Gel Formation for a Fluorinated Polymer Colloid. *Langmuir* **2005**, *21*, 2062-2077.

(38) Poon, W. C. K.; Haw, M. D. Mesoscopic structure formation in colloidal aggregation and gelation. *Adv. Colloid Interfac.* **1997**, *73*, 71-126.

(39) Fartaria, R.; Javid, N.; Pethrick, R. A.; Liggat, J. J.; Sefcik, J.; Sweatman, M. B. Structure of laponite-styrene precursor dispersions for production of advanced polymer-clay nanocomposites. *Soft Matter* **2011**, *7*, 9157-9166.

(40) Javid, N.; Vogtt, K.; Roy, S.; Hirst, A. R.; Hoell, A.; Hamley, I. W.; Ulijn, R. V.; Sefcik, J. Supramolecular Structures of Enzyme Clusters. *J. Phys. Chem. Lett.* **2011**, *2*, 1395-1399.

(41) Yamamoto, T.; Nishimura, T.; Suzuki, T.; Tamon, H. Control of mesoporosity by sol-gel polycondensation and freeze drying. *J. Non-Cryst. Solids* **2001**, *288*, 46-55.

(42) Pekala, R. W.; Kong, F. M. A synthetic route to organic aerogels – mechanism, structure, and properties. *J. Phys. (Paris)* **1989,** *50*, 33-40.

Scheme 1. Two-step polymerization process through the addition reaction of resorcinol and formaldehyde, followed by the subsequent polycondensation of the hydroxymethyl derivative. The initial reaction is shown with representative stoichiometry of 1:2, producing the di-substituted hydroxymethyl. Mono- and tri-substituted hydroxymethyl derivatives will also form but these are omitted for clarity.

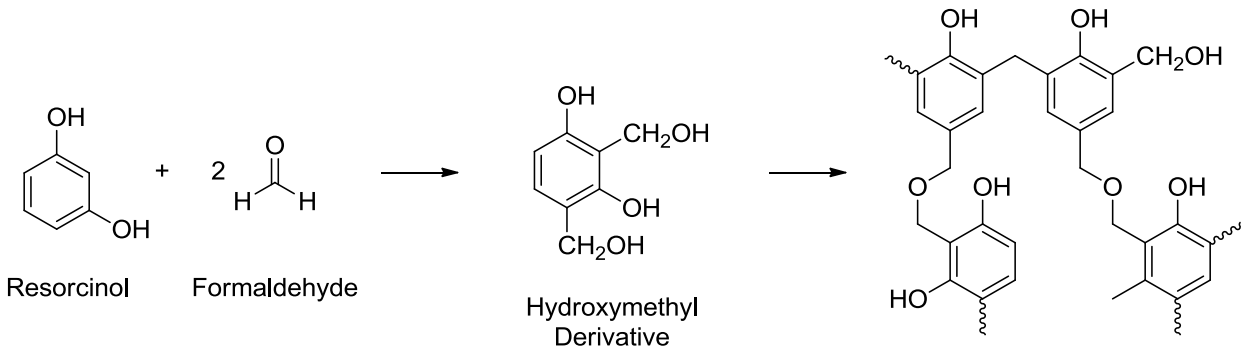

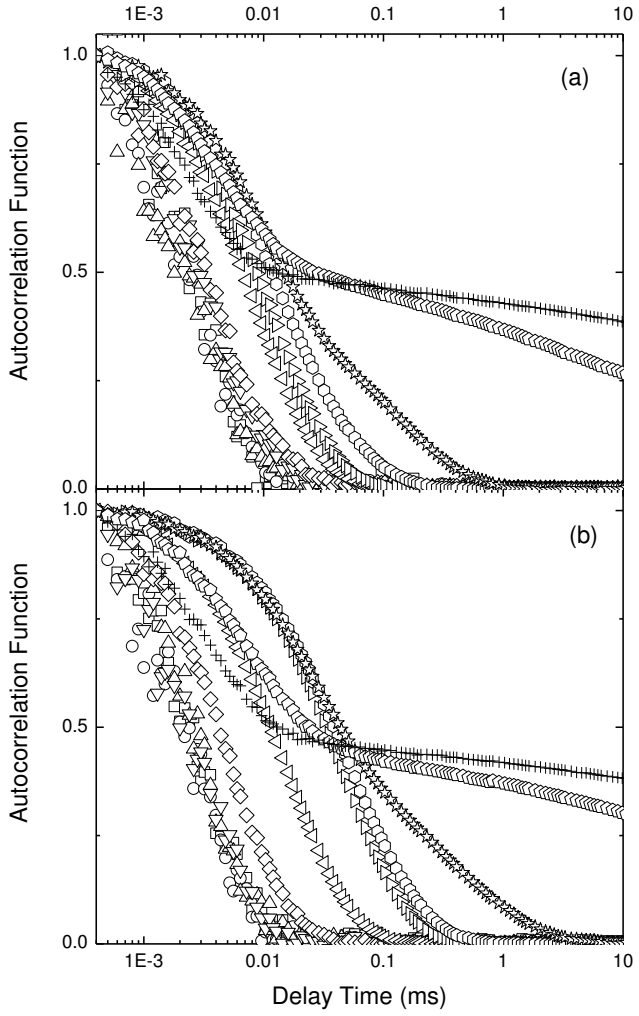

Figure 1. Autocorrelation function for (a) sodium carbonate and (b) cesium carbonate at R/C 100. Measurements are taken every 10 % of the total gel time such that (∀) 0 %, (–) 10 %, (8) 20 %, (X) 30 %, (M) 40 %, (Ξ) 50 %, (χ) 60 %, (ν) 70 %, (ψ) 80 %, (□) 90 % and (□) 100 %.

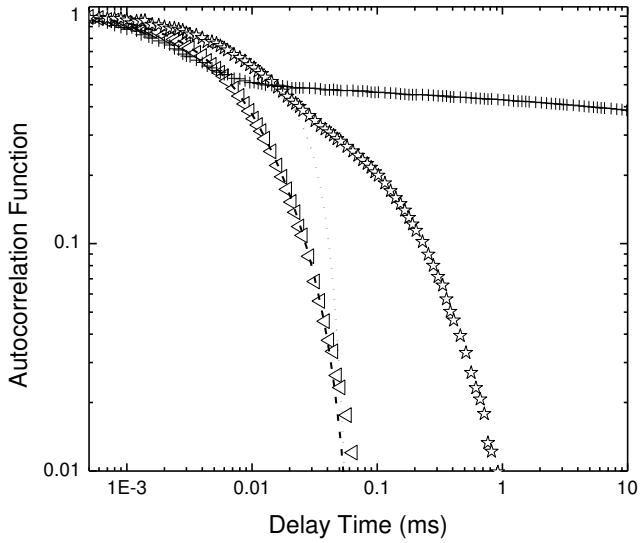

Figure 2. Autocorrelation functions for sodium carbonate R/C 100 at (Ξ) 50 %, (ψ) 80 % and (□) 100 %, illustrating the changing decay profile shape. Dashed lines represent the theoretical exponential decay of a monodisperse sample with hydrodynamic radius determined from the initial decay rate.

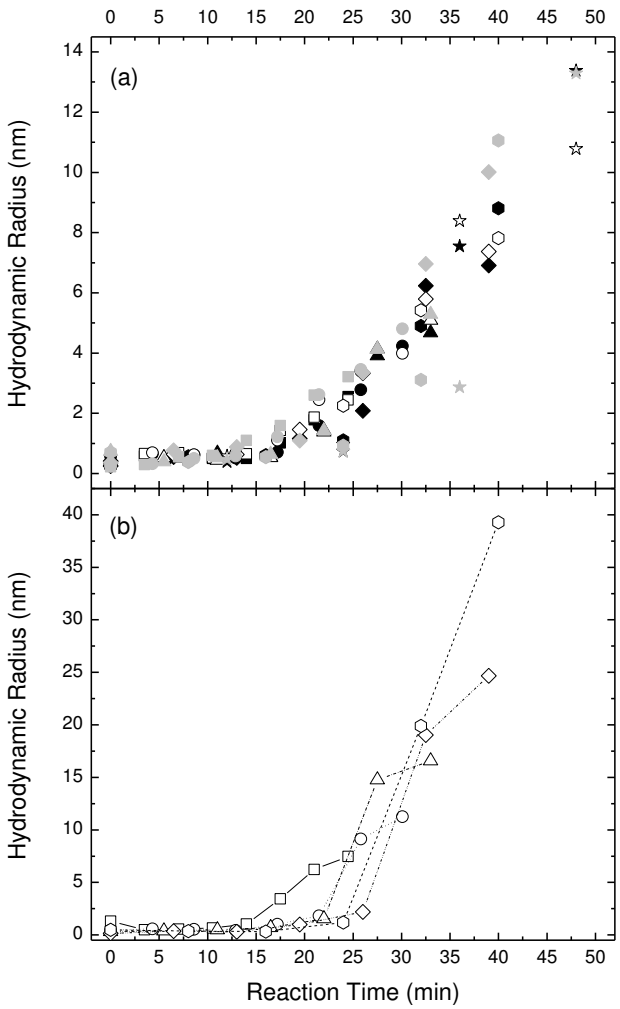

Figure 3. Hydrodynamic radii as determined from autocorrelation functions for (a) lithium carbonate (black symbols), sodium carbonate (open symbols) and potassium carbonate (grey symbols) and (b) cesium carbonate, at (∀) 100, (–) 200, (8) 300, (M) 400, (ν) 500 and (ψ) 600.

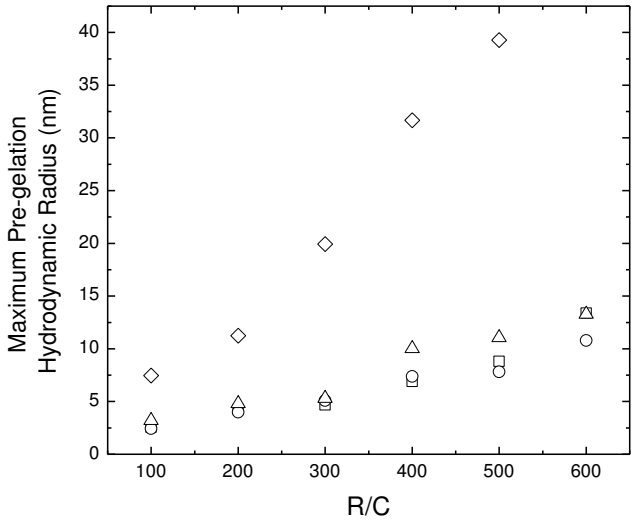

Figure 4. Maximum pre-gelation hydrodynamic radius as for determined for each R/C used for (∀) Li_2CO_3, (–) Na_2CO_3, (8) K_2CO_3 and (M) Cs_2CO_3.

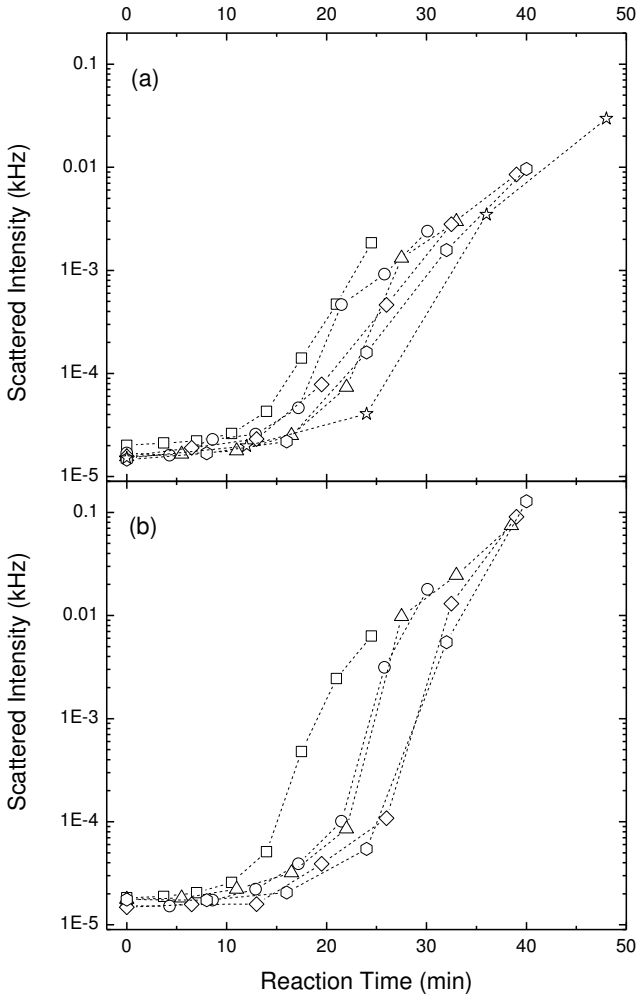
(a)
(b)
Scattered Intensity (kHz)
Scattered Intensity (kHz)
Reaction Time (min)
0.1
0.01
1E-3
1E-4
1E-5
0
10
20
30
40
50

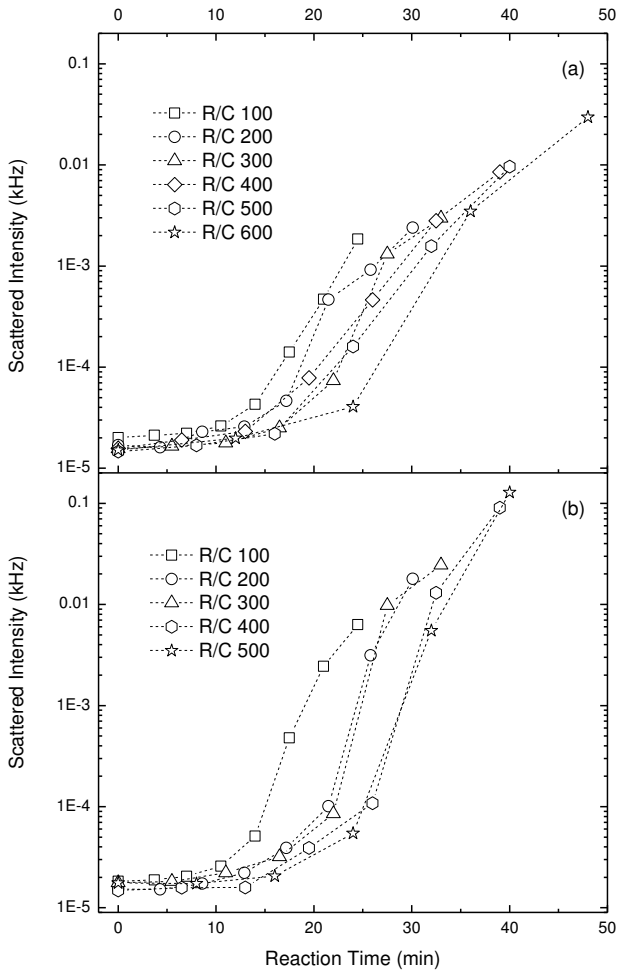

Figure 5. Scattered light intensities for (a) sodium carbonate and (b) cesium carbonate at R/C ratios of (∀) 100, (–) 200, (8) 300, (M) 400, (ν) 500 and (ψ) 600.

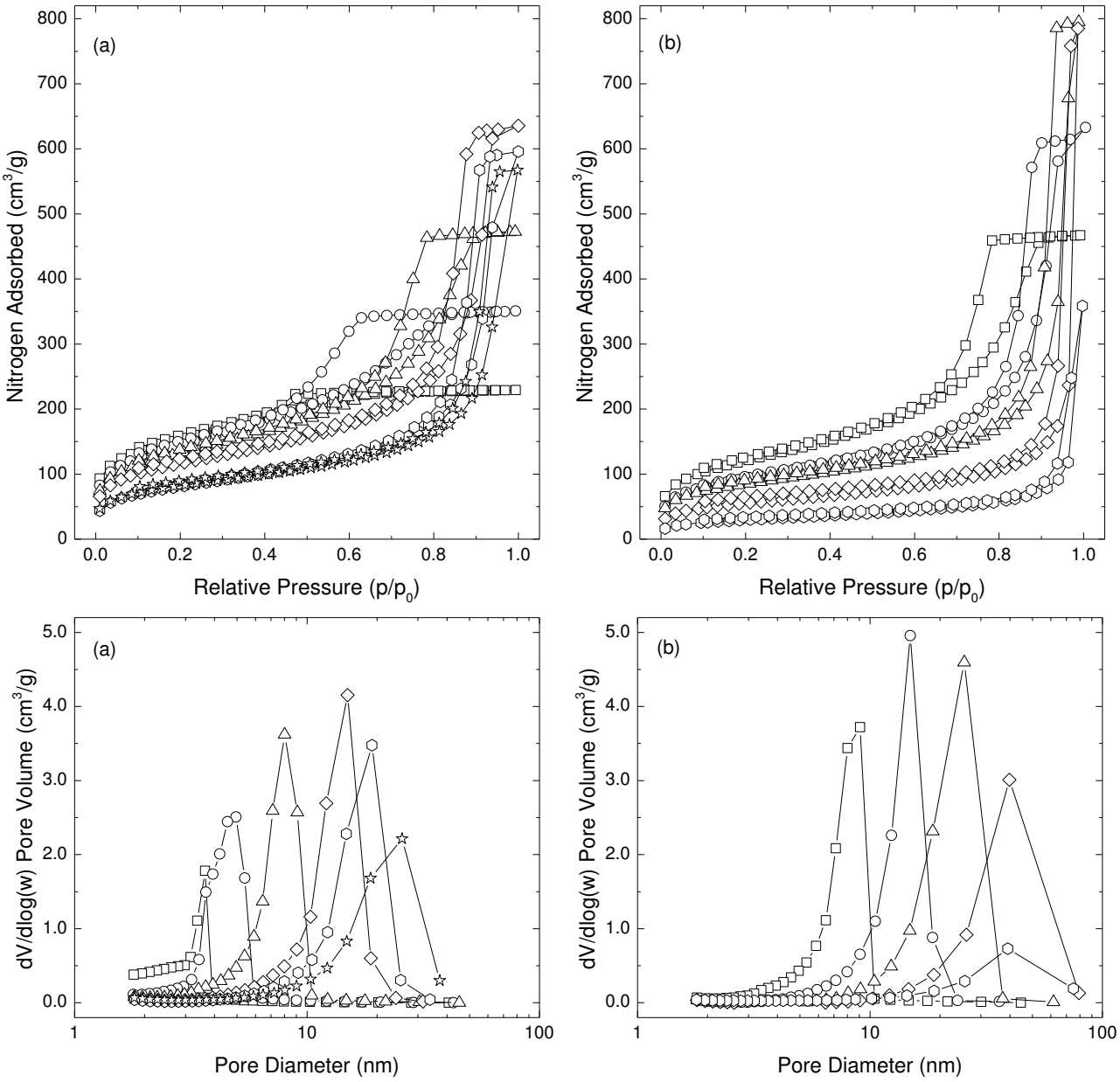

Figure 6. Adosrption/desorption isotherms (top) and pore size distributions (bottom) for (a) sodium carbonate and (b) cesium carbonate at R/C ratios of (∀) 100, (–) 200, (8) 300, (M) 400, (ν) 500 and (ψ) 600.

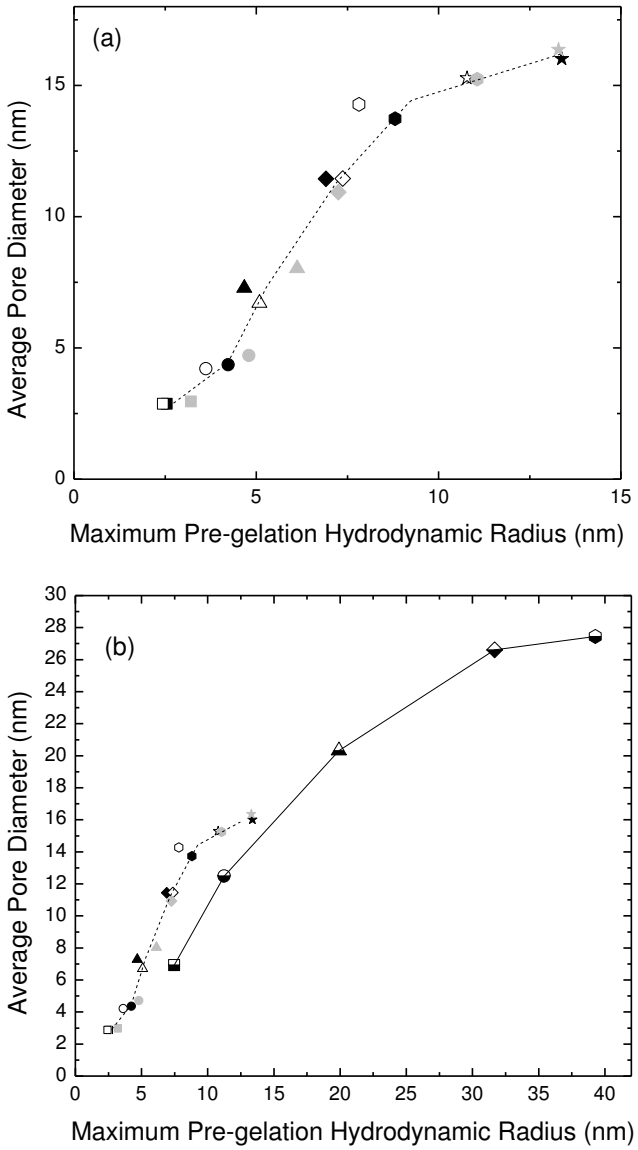

Figure 7. Master curve showing average pore diameter vs. maximum hydrodynamic radii for (a) lithium carbonate (black symbols), sodium carbonate (open symbols) and potassium carbonate (grey symbols)and (b) cesium carbonate (half-filled symbols) at R/C ratios of (∀) 100, (–) 200, (8) 300, (M) 400, (ν) 500 and (ψ) 600. Data from (a) is overlaid in (b) with reduced symbol size to allow for direct scale comparison.

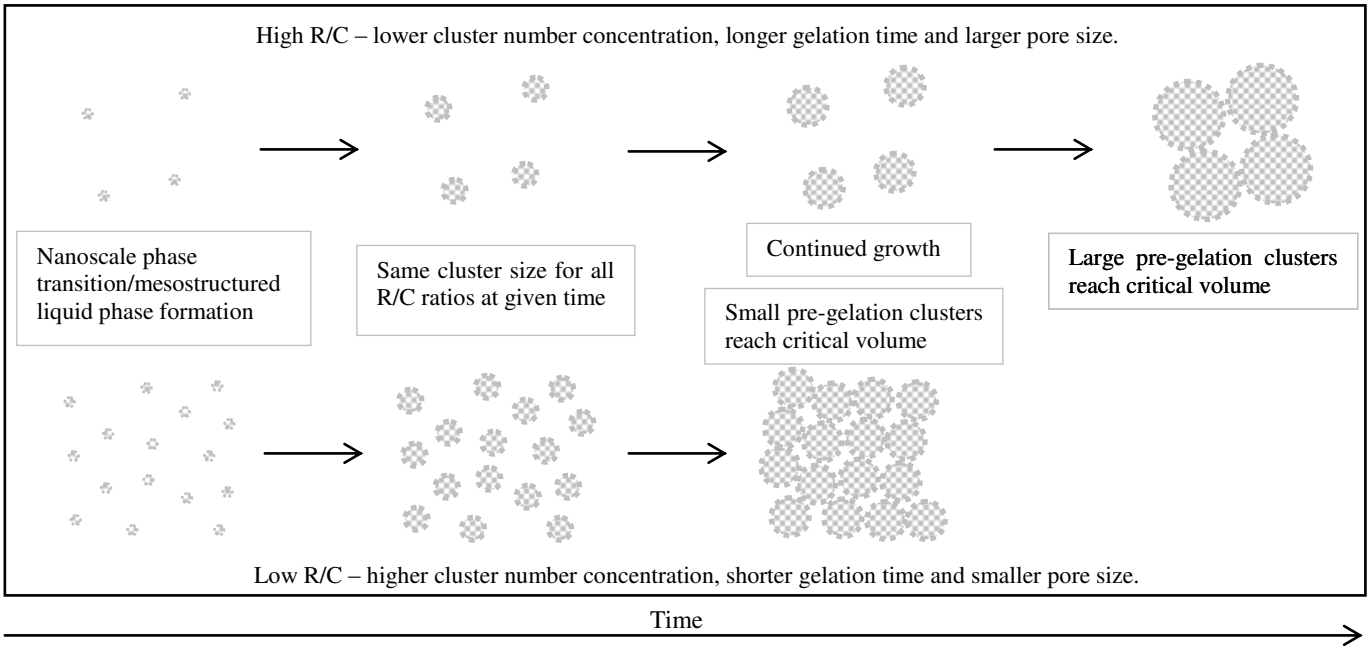

Figure 8. Schematic diagram outlining the cluster formation and growth process in resorcinol-formaldehyde gel synthesis. Clusters are depicted as spheres with sizes as indicated by DLS for clarity

Table 1. BET surface area (S_{BET}), BJH average pore size (d_p avg.) total pore volume (V_{Tot}) and initial pH for each dried gel sample.

		Li_2CO_3		
R/C	S_{BET} (m^2/g)[a]	d_P avg. (nm)	V_{Tot} (cm^3/g)	pH
100	527 ± 5	2.9	0.35	7.31
200	542 ± 4	4.4	0.59	7.07
300	498 ± 5	7.3	0.82	6.91
400	438 ± 5	11.4	1.05	6.85
500	376 ± 4	13.7	1.03	6.74
600	320 ± 4	16.0	1.00	6.65
		Na_2CO_3		
R/C	S_{BET} (m^2/g)[a]	d_P avg. (nm)	V_{Tot} (cm^3/g)	pH
100	533 ± 5	2.9	0.35	7.39
200	508 ± 4	4.2	0.54	7.09
300	461 ± 4	6.7	0.73	6.91
400	403 ± 4	11.5	0.98	6.84
500	284 ± 2	14.3	0.92	6.77
600	282 ± 4	16.5	0.88	6.66
		K_2CO_3		
R/C	S_{BET} (m^2/g)[a]	d_P avg. (nm)	V_{Tot} (cm^3/g)	pH
100	472 ± 4	3.0	0.33	7.36
200	554 ± 5	4.7	0.64	7.07
300	476 ± 5	7.9	0.85	6.92
400	465 ± 5	10.9	1.08	6.84
500	272 ± 2	15.2	0.94	6.75
600	299 ± 3	16.4	0.93	6.66
		Cs_2CO_3		
R/C	S_{BET} (m^2/g)[a]	d_P avg. (nm)	V_{Tot} (cm^3/g)	pH
100	425 ± 3	6.9	0.72	7.37
200	329 ± 3	12.6	0.98	7.09
300	293 ± 3	20.3	1.23	6.92
400	206 ± 2	28.0	1.15	6.85
500	103 ± 1	27.5	0.55	6.74

[a]All BET surface areas had a corresponding positive C value

Table of Contents Graphic